Identifying TeV source candidates among *Fermi*-LAT unclassified blazars

G. Chiaro,[1] M. Meyer,[2] M. Di Mauro,[3] D. Salvetti,[1] G. La Mura,[4] and D. J. Thompson[3]

[1]*Institute of Space Astrophysics & Cosmic Physics, INAF*
Via Bassini 15, I-20133 Milano Italy
[2]*Kavli Institute for Particle Astrophysics and Cosmology, Dpt. of Physics, SLAC,*
Stanford University, Stanford, California 94305, USA
[3]*NASA Goddard Space Flight Center*
Greenbelt, MD 20771 USA
[4]*Lab. de Instrumentacao e Fisica Experimental de Particulas. LIP*
Av. Gama Pinto 2, Lisboa, Portugal

ABSTRACT

Blazars and in particular the subclass of high synchrotron peaked Active Galactic Nuclei are among the main targets for the present generation of Imaging Atmospheric Cherenkov Telescopes (IACTs) and will remain of great importance for very high-energy γ-ray science in the era of the Cherenkov Telescope Array (CTA). Observations by IACTs, which have small fields of view, are limited by observing conditions; therefore, it is important to select the most promising targets in order to save observation time and consequently to increase the number of detections. The aim of this paper is to search for unclassified γ-ray blazars that are likely detectable with IACTs or CTA, using an artificial neural network algorithm and updated analysis of *Fermi* Large Area Telescope data. We found 80 γ-ray sources, and for these sources we study their light curves and, for the highest-confidence candidates, potential detectability by IACTs and/or CTA. Follow-up observations of our source candidates could significantly increase the current TeV source population sample and could ultimately confirm the efficiency of our algorithm to select TeV sources. It could also lead to a revision of the predicted number of sources that will be detected in the CTA extragalactic survey.

Keywords: gamma rays — blazars — catalogs — surveys

1. INTRODUCTION

Blazars, some of the most powerful Active Galactic Nuclei (AGNs), have a relativistic jet pointing toward the observer (e.g., Abdo et al. 2010; Massaro et al. 2015) and show rapid variability and high optical and radio polarization. Such objects are the most numerous class of extragalactic sources detected by TeV telescopes, the most sensitive of which are the Imaging Atmospheric Cherenkov Telescopes (IACTs) such as the existing MAGIC[1], H.E.S.S.[2], and VERITAS[3] facilities and the upcoming Cherenkov Telescope Array (CTA)[4]. Despite their high sensitivity, however, observations by current IACTs are limited by their small fields of view, weather conditions, the need for relatively dark night skies, and by a high background that requires fairly long observations. A source with a flux of $\sim$1% of the Crab nebula flux requires around 50 hours of observation time. IACTs typically take data for only about 1200 hours per year (De Naurois et al. 2015). Those constraints provide a strong incentive to identify likely targets for IACT observations.

Corresponding author: Graziano Chiaro
graziano.chiaro@inaf.it

[1] https://magic.mpp.mpg.de/
[2] https://www.mpi-hd.mpg.de/hfm/HESS/
[3] https://veritas.sao.arizona.edu/
[4] https://www.cta-observatory.org/

The all-sky observations with the Large Area Telescope (LAT) on the *Fermi Gamma-ray Space Telescope (Fermi)* (Atwood et al. 2009) at GeV energies offer opportunities to find such targets. An example is the Third Catalog of Hard *Fermi*-LAT Sources (3FHL: Ajello et al. 2017), which reports the locations and spectra of sources significantly detected in the 10 GeV - 2 TeV energy range during the first 7 years of the *Fermi* mission. From the 3FHL it is possible to select TeV candidates by γ-ray flux and spectral index.

An alternative approach to searching for TeV candidates is to find objects belonging to a class of sources likely to be seen at TeV energies. In the case of blazars, this can be done by identifying those objects whose synchrotron emission peaks at high frequencies. Blazar Spectral Energy Distributions (SEDs) show broad humps in a νf_ν representation. The low-energy hump is attributed to synchrotron radiation, and the high-energy one is usually thought to be due to inverse Compton radiation (IC) (e.g. Ghisellini 2013). Based on the position of the peak of the synchrotron hump (ν_{peak}^S) in the SED, blazars are divided into three subclasses: low-synchrotron-peaked (LSP, with $\nu_{peak}^S \leq 10^{14}$ Hz), intermediate-synchrotron-peaked (ISP, with 10^{14} Hz $< \nu_{peak}^S \leq 10^{15}$ Hz) and high-synchrotron-peaked (HSP, with $\nu_{peak}^S > 10^{15}$ Hz) (Abdo et al. 2010). HSPs, primarily BL Lac objects, represent the most numerous class of extragalactic TeV-energy sources. The TeVCat[5] is an online, interactive catalog for very-high-energy (VHE energies, $E > 100$ GeV) γ-ray astronomy (Horan et al. 2008). This catalog reports 223 TeV sources, where 51 of them are HSPs and only 10 are LSP/ISP flat-spectrum radio quasars (FSRQs).[6] An example of searching out HSP candidates is the second *WISE* High Synchrotron Peak Catalog (2WHSP) (Chang et al. 2017), which is an independent list of HSP candidates based on the multi-frequency analysis of γ-ray source candidates away from the Galactic Plane.

The present search for TeV HSP source candidates is a third approach, using a two-step method: (1) We use γ-ray variability information to search out potential HSPs among the unclassified *Fermi*-LAT sources; and (2) We analyze γ-ray spectra of these sources using more *Fermi*-LAT data than are available in published catalogs. The starting point is the third *Fermi*-LAT all-sky catalog of sources detected at energies between 100 MeV and 300 GeV (3FGL: Acero et al. 2015). The 3FGL catalog lists 3033 γ-ray sources, of which 1745 are AGNs, mostly BL Lacs and FSRQs, and includes γ-ray source locations, energy spectra, variability information on monthly time scales, and likely associations with objects seen at other wavelengths. In this catalog 573 sources are listed as blazars of uncertain type (BCUs) and 1010 objects are unassociated with a plausible counterpart at other wavelengths (UCSs).[7]

Although BCUs and UCSs often lack optical spectra and sufficient information for a rigorous classification, statistical methods such as the Artificial Neural Network (ANN) algorithm can potentially provide classifications of these sources (e.g., Chiaro et al. 2016; Saz Parkinson et al. 2016; Salvetti et al. 2017; Lefaucheur et al. 2017). In particular, Saz Parkinson et al. (2016) found 559 of the UCS sources have characteristics similar to those of AGN. These UCS$_{agns}$ are combined with the original 573 BCUs from the 3FGL catalog to provide the targets for our search for HSP/TeV candidates. The paper is organized as follows: in Sect. 2 we present the machine learning method used in this study; in Sect. 3 we describe the selection of HSP candidates among the uncertain 3FGL objects; and in Sect. 4 we discuss the results of a dedicated *Fermi*-LAT analysis of the sources found analyzing 104 months of data. In Sect. 5 we examine the detectability of the targets by the present generation of IACTs and CTA. In Sect. 6 we discuss the results of this study.

2. THE ANN SEARCH METHOD

The starting point for selecting HSP candidates is the ANN method previously applied to *Fermi*-LAT sources to distinguish FSRQ-like sources from those with BL Lac characteristics (Chiaro et al. 2016; Salvetti et al. 2017). This approach uses the two-layer-perceptron ANN technique (Gish 1990), which is probably the most widely used architecture for practical applications of neural networks. We applied the algorithm to the three synchrotron peak subclasses as classified in the Third Catalog of Active Galactic Nuclei detected by the *Fermi* LAT (3LAC: Ackermann et al. 2015) in order to train it to distinguish each source class on the basis of their monthly $E > 100$ MeV γ-ray flux values. The algorithm computes a likelihood value arranged to have two possibilities: class A or class B, with a likelihood (L) assigned to each analyzed source so the likelihoods to belong to either of the two classes are related by $L_A = 1 - L_B$. In this way, the greater the value of L_A, the greater the likelihood that the source is a class A candidate. In this case, the Likelihood applies to the source having HSP characteristics, L_{HSP}.

---

[5] http://tevcat.uchicago.edu/

[6] The rest of the sources in TeVCat are Galactic sources or of unidentified nature.

[7] A preliminary version of the 4FGL catalog is available at https://fermi.gsfc.nasa.gov/ssc/data/access/lat/8yr_catalog/, but it does not include the variability information needed for this analysis.
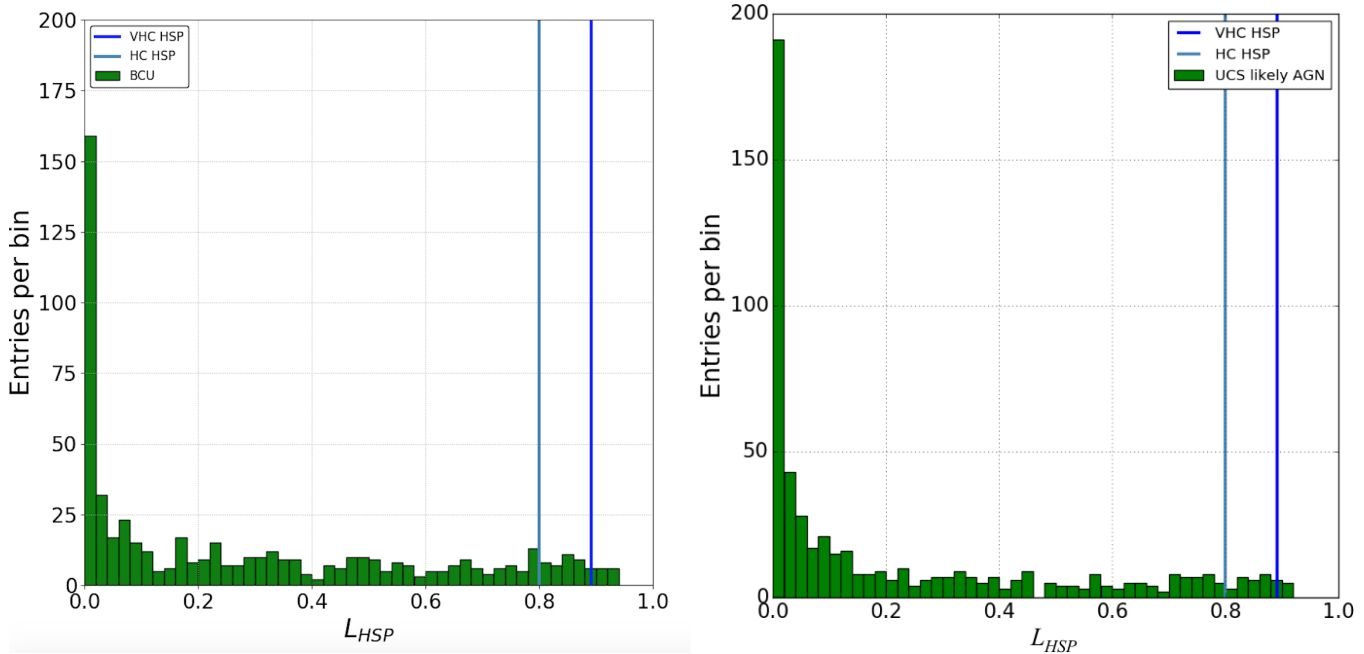
Figure 1. ANN likelihood to be HSP candidates of 3FGL BCUs (left) and UCS$_{agn}$ (right). Vertical blue and steel blue lines indicate the classification thresholds of our ANN algorithm to identify sources with a $L_{HSP} > 0.8$ and VHC candidates with $L_{HSP} > 0.89$.

Repeating the analysis of Chiaro et al. (2016), we considered 289 HSPs and 824 non-HSP objects classified in the 3LAC catalog. Maintaining the same ratio as in the catalog, that is, one third HSPs and two thirds non-HSP sources, we randomly mixed the sample and divided it into 3 subsamples: training, validation, and testing. The training sample is used to optimize the network. The validation sample is used to avoid over-fitting. The testing sample is independent both of the training and validation ones and was used to monitor the accuracy of the network. Although the random sampling resulted in a different training set from the previous analysis, the results were the same: for $L_{HSP} > 0.8$, 75% of the sources have characteristics of HSPs, while for $L_{HSP} > 0.89$, we expect 90% of the sources to be HSP-like.

3. IDENTIFYING HSP CANDIDATES

We applied the ANN HSP algorithm to the 573 BCUs and the 559 UCS$_{agn}$ of our sample. The resulting likelihood distributions show, as expected, a peak at $L_{HSP} = 0.0$ due to the non-HSP populations (ISP and LSP), which are much more numerous than HSPs (Fig. 1). The lack of a peak at $L_{HSP} = 1.0$ indicates that the ANN network was not able to separate HSPs cleanly, but for the purpose of selecting candidates for additional analysis we are primarily interested in finding a high fraction of the sources with the desired characteristics. Requiring the $L_{HSP} > 0.8$ value, we identified 48 BCU and 32 UCS$_{agn}$ as HSP candidates. Applying the higher threshold value $L_{HSP} > 0.89$, we identified 11 BCUs and 5 UCS$_{agn}$ as Very High Confidence (VHC) HSP candidates. Table 1 and Table 2 show the full lists of candidates, where the VHC sources are on the top of the list.

4. FERMI-LAT SPECTRAL ANALYSIS

We analyzed 104 months of *Fermi*-LAT Pass 8 (Atwood et al. 2013) data from 2008 August 4 to 2017 April 4, selecting γ-ray events in the energy range $E = [0.1, 1000]$ GeV, passing standard data quality selection criteria, in order to find the γ-ray properties of our HSP candidates. We considered events belonging to the Pass 8 SOURCE event class and used the corresponding instrument response functions P8R2_SOURCE_V6, since we were interested in point source detection. We used the interstellar emission model (IEM) released with Pass 8 data (Acero et al. 2016) (i.e.,

`gll_iem_v06.fits`). This is the model routinely used in Pass 8 analyses. We also included the standard template for the isotropic emission (`iso_P8R2_SOURCE_V6_v06.txt`) [8].

We developed an analysis pipeline using `FermiPy`, a Python package that automates analyses with the *Fermi* Science Tools (Wood M. 2017)[9]. `FermiPy` includes tools that can 1) generate simulations of the γ-ray sky, 2) detect point sources, and 3) calculate the characteristics of their SEDs. For more details on `FermiPy` we refer to the Appendices of Ajello et al. (2017). The likelihood analysis works on a square region of interest (ROI). We used a $16° \times 16°$ ROI centered on the sources of our sample. We analyzed each ROI separately. In each ROI, we binned the data with a pixel size of $0.08°$ and 8 energy bins per decade. Our model includes the IEM, isotropic template and sources from the preliminary 8-year list[10]. We allowed the normalization and slopes of the IEM and isotropic templates to vary. We first relocalized the source of interest, and then we searched for new point sources with Test Statistic $TS > 25$, defined as twice the difference between the log-likelihood for the null hypothesis (no source) and the hypothesis of a source at the location. We apply a power-law SED for the sources in our sample. After this first step we calculate the SED of the source and we compute its lightcurve in order to determine whether the source is variable. The variability was estimated for each source by calculating the Test Statistic for variability (TS_{VAR}), defined as twice the difference between the log-likelihood for the null hypothesis (constant flux in time) and the hypothesis of a variable flux.

In Table 3 and Table 4 we report the following parameters for the HSP candidates: the best fit and 1σ error of the position, the TS of detection, the pivot energy (i.e. energy at which error on differential flux is minimal), the spectral index found for a power-law SED shape, the flux and energy flux integrated between 100 MeV to 300 GeV. The spectral index parameter, if less than 2, can be a relevant indicator for an IC peak at TeV energies and therefore quite useful in selecting IACT or CTA candidates. The mean and rms of the spectral indexes of HSPs are 1.87 ± 0.20 while for LSPs and ISPs these are 2.21 ± 0.18, 2.07 ± 0.20 respectively.

5. TEV CANDIDATES

In this section, we compare the extrapolated fluxes of these sources against the sensitivity of present IACTs and the future CTA. We use the *Fermi*-LAT spectral shapes obtained in the previous section and focus further analysis on the VHC candidates. In order to evaluate whether the VHC HSP candidates can realistically be observed with IACTs or CTA, we must take into account the interaction of γ-rays with photons of the extragalactic background light (EBL). The relevant part of the EBL spans the wavelength regime from ultraviolet to far-infrared wavelengths and mainly consists of the integrated starlight emitted over the history of the Universe and starlight absorbed and re-emitted by dust in galaxies (Hauser et al. 2001; Kashlinsky et al. 2005). During the propagation of γ rays through the EBL, the electron-positron pairs produced via $\gamma\gamma \rightarrow e^{+}e^{-}$ leads to an attenuation of the initial γ-ray flux (Nikisov et al. 1962; Gould et al. 1967; Dwek et al. 2013). To properly evaluate the absorption effect of the EBL it is necessary to know the redshift of the analyzed γ-ray source. Since the redshifts of the selected VHC candidates are unknown, we assume redshifts between $z = 0$ and $z = 0.5$, which are typical values of observed BL Lacs. We used these z values while recognizing that blazar redshift range is a very open and long standing debate. Some authors argue that the BL Lacs without a redshift are likely much more distant than those with a measured one (e.g., Padovani et al. 2012), so it could be possible that some objects fall beyond the 0-0.5 redshift range. Using the EBL model of Dominguez et al. (2011), we extrapolate the best-fit spectra obtained with the *Fermi* analysis in Sec. 4 up to 10 TeV with the assumed redshift values. The results are shown in Fig. 2 and Fig. 3 where we compare the extrapolated fluxes with the CTA sensitivity for 50 hours (5 hours) of observations as a solid (dashed) gray line. The CTA sensitivity curves are available for the northern and southern array and for zenith angles, Z, of $20°$ and $40°$. We choose the sensitivity curve depending on the source declination δ assuming CTA site locations at $28.7°$ northern latitude and $24.7°$ southern latitude. For $\delta > 58.7°$, we choose the northern array with $Z = 40°$, for $58.7° \leqslant \delta < 2.7°$ the northern array with $Z = 20°$, for $2.7 \geqslant Z \geqslant -54.7°$ the southern array with $Z = 20°$, and the southern array with $Z = 40°$ for $\delta < -54.7°$.[11] The CTA sensitivity for 5 hours of observation is similar to that of currently operating IACTs for 50 hours of observation, although the current IACTs have typically a higher threshold energy of $\gtrsim 80$ GeV. For a redshift of $z = 0.5$ most of the considered sources should still be detectable by currently operating IACTs and appear to be good candidates for detection with CTA. In Table 5, we report the maximum redshift values of the TeV

---

[8] For descriptions of these templates, see http://fermi.gsfc.nasa.gov/ssc/data/access/lat/BackgroundModels.html.

[9] See http://fermipy.readthedocs.io/en/latest/.

[10] https://fermi.gsfc.nasa.gov/ssc/data/access/lat/fl8y/gll_psc_8year_v5.fit

[11] The sensitivity curves of the northern and southern array are available at www.cta-observatory.org

candidates so that the sources are still detectable at $5\,\sigma$ for 5- and 50-hour CTA observations. If no value is given, the source will not be significantly detected with the assumed observation time at any redshift.

6. CONCLUSIONS

Motivated by wishing to expand the sample of TeV sources, we applied a machine learning algorithm to variability parameters of *Fermi*-LAT blazar-like sources without firm identifications combined with new analysis of the LAT data for these sources. Follow-up work will necessitate additional multiwavelength studies, including finding redshifts for most of the candidates and targeted observation by IACTs. We also recognize that this search is necessarily incomplete because of the difficulty to distinguish the blazar subclasses by the γ-ray **flux** properties only. As already pointed out by Ackermann et al. (2015), the γ-ray sources with unknown properties are generally fainter than the well-defined classes. The fainter sources offer less of the variability information needed for the machine learning method, and so there may be HSP blazars among the sample 3FGL sources rejected in the first step of our method. The level of incompleteness is difficult to quantify due to the very similar values of the synchrotron peaks of the three blazar subclasses. Nevertheless, the VHC HSP candidates, also thanks to the analysis of *Fermi*-LAT data, are convincing as TeV candidates and could be promising targets for CTA observations for population studies.

7. ACKNOWLEDGMENTS

Facilities: *Fermi*, HST(STIS), Swift(XRT and UVOT), AAVSO, CTIO:1.3m, CTIO:1.5m,CXO

REFERENCES

Abdo A.A. , Ackermann M., Agudo I. et al., 2010, ApJ, 716,30

Acero F., Ackermann, M., Ajello M. et al. , 2015, ApJS, 218, 23

Acero F., Ackermann, M., Ajello M. et al. , 2016, ApJS, 223, 26

Ackermann, M., Ajello, M., Atwood W.B. et al., 2015, ApJ 810, 14, 34

Aharonian A. , Akhperjanian A., Bazer-Bachi A. et al., 1993, ExA, 2, 331

Ajello M., Atwood W. B.,Baldini L. et al., 2017, ApJS, 232, 18

Ajello, M. , Baldini L., Ballet J. et al., 2017, ArXiv: 1705.00009

Alvarez Crespo N., Masetti N., Ricci F. et al., 2016 AJ, 151, 32

Ambrogi L. , Celli S., Aharonian A. et at., 2018, APh, 69 , 79

Angioni R. , Grandi P., Torresi E. et al., 2017, APh, 92,42

Arsioli B., Chang Y., 2017, A&A, 598, 134

Arsioli B., Giommi P.,Fragon B. et al, 2015, A&A, 579, 34

Atwood W. B. , Abdo A. A., Ackermann M. et al., 2009, ApJ, 697, 1071

Atwood, W., Albert, A., Baldini, L., et al. 2013, eConf C121028, 8, in Proc. 4th Fermi Symposium, Monterey

Table 1. Full list of BCU HSP candidates. Columns: (1) 3FGL name; (2) Association with known source; (3) Included in 2WHSP catalog; (4) Detection TS 0.1– 300 GeV; (5) Variability TS_{VAR}; (6) HSP Likelihood. At the top of the list are the VHC sources ($L > 0.89$).

| 3FGL name	Association	2WHSP	TS	TS_{VAR}	L_{HSP}
3FGL J0047.9+5447	1RXS J004754.5+544758		56.7	11.7	0.92
3FGL J1155.4-3417	NVSS J115520-341718	⋄	147.3	16.2	0.92
3FGL J1434.6+6640	1RXS J143442.0+664031		73.9	16.7	0.92
3FGL J0921.0-2258	NVSS J092057-225721	⋄	62.5	10.5	0.91
3FGL J0648.1+1606	1RXS J064814.1+160708		40.1	13.9	0.90
3FGL J1711.6+8846	1RXS J171643.8+884414	⋄	44.3	12.4	0.90
3FGL J1714.1-2029	1RXS J171405.2-202747	⋄	73.8	18.1	0.90
3FGL J1910.8+2855	1RXS J191053.2+285622		102.2	15.1	0.90
3FGL J0153.4+7114	TXS 0149+710		80.8	19.7	0.89
3FGL J0506.9-5435	1ES 0505-546	⋄	455.4	29.8	0.89
3FGL J1944.1-4523	1RXS J194422.6-452326	⋄	100.6	11.1	0.89
3FGL J0742.4-8133c	SUMSS J074220-813139		32.2	11.8	0.88
3FGL J0043.7-1117	1RXS J004349.3-111612	⋄	69.4	12.5	0.88
3FGL J1824.4+4310	1RXS J182418.7+430954	⋄	80.9	19.7	0.88
3FGL J0528.3+1815	1RXS J052829.6+181657		35.6	14.6	0.87
3FGL J0646.4-5452	PMN J0646-5451		190.3	17.3	0.87
3FGL J0040.3+4049	B3 0037+405	⋄	75.9	12.0	0.87
3FGL J1959.8-4725	SUMSS J195945-472519	⋄	923.7	94.3	0.87
3FGL J2108.6-8619	1RXS J210959.5-861853	⋄	91.0	10.7	0.87
3FGL J0039.0-2218	PMN J0039-2220	⋄	89.3	11.6	0.86
3FGL J0305.2-1607	PKS 0302-16		147.6	22.9	0.86
3FGL J1040.8+1342	1RXS J104057.7+134216	⋄	69.1	11.0	0.86
3FGL J2312.9-6923	SUMSS J231347-692332	⋄	35.3	16.1	0.86
3FGL J0515.5-0123	NVSS J051536-012427		45.6	11.7	0.85
3FGL J0620.4+2644	RX J0620.6+2644	⋄	92.0	15.1	0.85
3FGL J0640.0-1252	TXS 0637-128	⋄	174.1	14.4	0.85
3FGL J0733.5+5153	NVSS J073326+515355	⋄	104.3	11.1	0.85
3FGL J1141.2+6805	1RXS J114118.3+680433		140.0	23.3	0.85
3FGL J1203.5-3925	PMN J1203-3926	⋄	103.2	18.5	0.85
3FGL J1939.6-4925	SUMSS J193946-492539		64.5	15.9	0.85
3FGL J2316.8-5209	SUMSS J231701-521003		37.3	15.1	0.85
3FGL J0132.5-0802	PKS 0130-083		71.9	12.4	0.8
3FGL J0342.6-3006	PKS 0340-302		43.1	13.3	0.8
3FGL J1446.8-1831	NVSS J144644-182922	⋄	27.9	8.6	0.84
3FGL J1855.1-6008	PMN J1854-6009		21.3	6.7	0.84
3FGL J0043.5-0444	1RXS J004333.7-044257	⋄	75.9	11.9	0.83
3FGL J0746.9+8511	NVSS J074715+851208	⋄	118.9	18.3	0.83
3FGL J0650.5+2055	1RXS J065033.9+205603		206.2	20.0	0.82
3FGL J1319.6+7759	NVSS J131921+775823		182.6	25.1	0.82
3FGL J1908.8-0130	NVSS J190836-012642		306.4	35.5	0.82
3FGL J2347.9+5436	NVSS J234753+543627		163.0	21.7	0.82
3FGL J0204.2+2420	B2 0201+24		27.6	12.	0.81
3FGL J0439.6-3159	1RXS J043931.4-320045	⋄	119.8	24.9	0.81
3FGL J1547.1-2801	1RXS J154711.8-280222		96.7	16.7	0.81
3FGL J1612.4-3100	NVSS J161219-305937	⋄	494.9	116.1	0.81
3FGL J0030.2-1646	1RXS J003019.6-164723	⋄	168.7	30.1	0.80
3FGL J1158.9+0818	RX J1158.8+0819	⋄	51.4	11.8	0.80
3FGL J1841.2+2910	MG3 J184126+2910	⋄	195.9	22.8	0.80
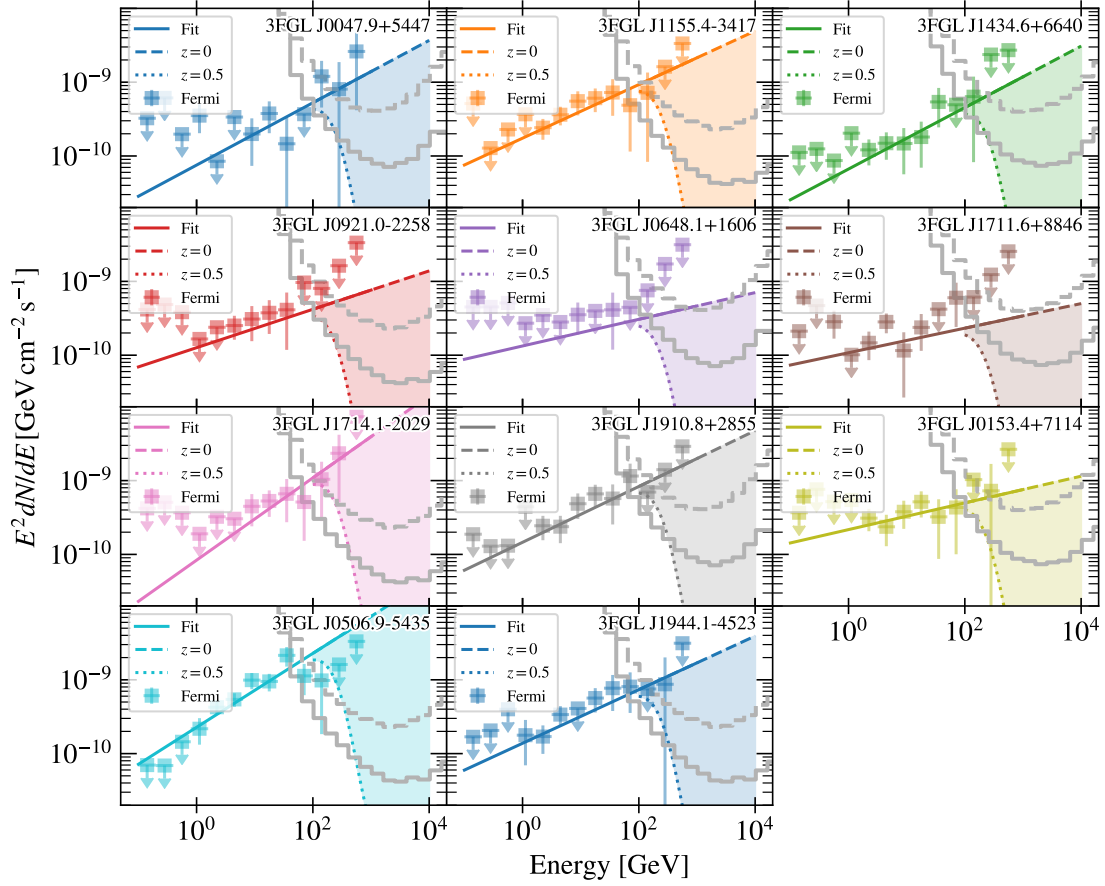
Figure 2. SEDs of the VHC BCU sources as TeV candidates. The dashed (dotted) line denotes the extrapolation of the best-fit spectra up to 10 TeV for a redshift of $z = 0$ ($z = 0.5$) The shaded region indicates the possible source flux for redshifts between $0 < z \leq 0.5$. The CTA sensitivity for 5 (50) hours of observation is shown as a gray dashed (solid) line.

Table 2. Full list of UCS$_{agn}$ HSP candidates. Columns: (1) 3FGL name; (2) Included in 2WHSP; (3) Detection TS 0.1– 300 GeV; (4) Variability TS_{VAR}; (5) HSP Likelihood. At the top of the list are the VHC sources ($L > 0.89$).

3FGL name	2WHSP	TS	TS_{VAR}	L_{HSP}
3FGL J1549.9-3044		64.2	10.1	0.91
3FGL J2142.6-2029		36.0	8.1	0.91
3FGL J2321.6-1619		34.1	45.1	0.91
3FGL J2145.5+1007		52.5	19.9	0.90
3FGL J2300.0+4053		174.5	6.9	0.90
3FGL J1155.3-1112		52.4	11.3	0.89
3FGL J2224.4+0351		29.5	9.5	0.89
3FGL J1525.8-0834	◇	59.5	23.2	0.89
3FGL J1619.1+7538		107.1	14.9	0.88
3FGL J0251.1-1829		104.2	10.2	0.88
3FGL J0020.9+0323		60.6	22.5	0.88
3FGL J0813.5-0356		57.0	13.1	0.88
3FGL J1234.7-0437		51.5	29.7	0.87
3FGL J1922.2+2313		80.8	22.6	0.87
3FGL J2043.6+0001		48.4	24.4	0.87
3FGL J0312.7-2222		177.1	18.2	0.87
3FGL J1513.3-3719	◇	54.7	18.0	0.87
3FGL J0524.5-6937		94.1	18.3	0.86
3FGL J1225.4-3448		22.2	7.0	0.86
3FGL J1222.7+7952		43.8	14.7	0.86
3FGL J2309.0+5428	◇	77.0	17.6	0.85
3FGL J2015.3-1431	◇	17.4	14.6	0.85
3FGL J2053.9+2922		359.6	43.9	0.85
3FGL J0234.2-0629		90.7	20.7	0.84
3FGL J1545.0-6641		150.1	11.8	0.84
3FGL J0731.8-3010		37.0	12.9	0.84
3FGL J0952.8+0711		50.9	14.1	0.84
3FGL J0527.3+6647		51.8	14.7	0.83
3FGL J1528.1-2904		26.2	11.7	0.83
3FGL J0049.0+4224	◇	36.9	16.5	0.82
3FGL J1057.6-4051	◇	40.2	15.5	0.82
3FGL J0928.3-5255		98.7	26.6	0.80

Bishop C.M., Neural Network for Pattern Recognition, 1995

Carosi A. , 2015, Proceeding of the 34th International Cosmic Ray Conference, p. 5

Chang Y.L. , Arsioli B., Giommi P. et al. , 2017, A&A , 598, 17

Chiaro G. , D.Salvetti, G. La Mura et al., 2016 MNRAS 462.3.3180C

Costamante L. , 2002, A&A, 384, 56

De Naurois M., Mazin D. , 2015, Comptes rendus - Physique, 16, 610

De Naurois M, Rolland L. , 2009, Aph, 32, 331

Doert M. , Errando M., 2014, ApJ, 782, 41

Dwek E. , Krennrich F. , 2013, APh, 43,112

Dominguez A. , Primack J. R.; Rosario D. J. et al.,2011, MNRAS, 410, 2556

Ghisellini G., 2013, EPJ Web of Conference, Vol. 61, id.05001.

Gish H., 1990, Proceeding on Acoustic Speech and Signal Processing, p. 1361

Gould R., Schreder G.,1967, Ph Rv, 155, 1408

Hassan T., Dominguez A., Leufaucher J. et al, 2013, arxiv 1708.0774

Hauser M., DweK E. , 2001,ARAA, 2001,39,249

Hillas A.M. , Akerlof, C. W., Biller, S. D et al., 1998, ApJ, 503, 744

Horan D., Wakeley S., 2008, AAS, HEAD meeting 10, id.41.06

Table 3. Results of the *Fermi*-LAT analysis of the full list of BCU HSP candidates. Columns: (1) 3FGL name; (2) RA; (3) DEC; (4) 68% error on the position; (5) Detection TS 0.1– 300 GeV; (6) Pivot energy; (7) Spectral Index; (8) Flux in the energy range 0.1– 300 GeV; 9) Energy flux in the energy range 0.1– 300 GeV

| 3FGL name	RA	DEC	pos_{68}%	TS	Pivot Energy	Sp.Index	Flux	Energy Flux
	[deg]	[deg]	[deg]		MeV		[10^{-9} ph/cm^2/s]	[10^{-6} MeV/cm^2/s]
3FGL J0030.2-1646	7.59	-16.82	0.02	168.7	5255	1.66 ± 0.08	13.4 ± 3.3	5.7 ± 1.5
3FGL J0039.0-2218	9.77	-22.32	0.03	89.3	5338	1.67 ± 0.11	9.2 ± 2.9	3.7 ± 1.2
3FGL J0040.3+4049	10.09	40.83	0.03	75.9	5638	1.92 ± 0.16	18.2 ± 9.4	2.3 ± 0.6
3FGL J0043.5-0444	10.88	-4.72	0.04	54.0	4015	1.91 ± 0.15	16.2 ± 7.2	2.1 ± 0.6
3FGL J0043.7-1117	10.94	-11.31	0.04	69.4	3405	1.86 ± 0.12	16.0 ± 5.3	2.6 ± 0.8
3FGL J0047.9+5447	12.02	54.81	0.03	56.7	19002	1.58 ± 0.16	4.9 ± 3.2	3.2 ± 1.3
3FGL J0132.5-0802	23.19	-8.07	0.03	71.9	3213	1.87 ± 0.11	16.8 ± 5.4	2.5 ± 0.7
3FGL J0153.4+7114	28.43	71.26	0.02	80.9	6435	1.82 ± 0.13	17.5 ± 7.3	3.4 ± 0.9
3FGL J0204.2+2420	31.09	24.27	0.04	27.6	7321	1.70 ± 0.16	4.7 ± 2.6	1.6 ± 0.8
3FGL J0305.2-1607	46.29	-16.14	0.02	147.6	4906	1.80 ± 0.11	17.8 ± 5.8	3.8 ± 1.0
3FGL J0342.6-3006	55.71	-30.11	0.04	43.2	2633	1.96 ± 0.14	12.5 ± 4.7	1.3 ± 0.4
3FGL J0439.6-3159	69.85	-32.03	0.03	119.9	4973	1.75 ± 0.09	13.3 ± 3.9	3.6 ± 1.0
3FGL J0506.9-5435	76.76	-54.60	0.01	455.4	6916	1.50 ± 0.05	14.2 ± 2.2	14.3 ± 2.7
3FGL J0515.5-0123	78.87	-1.42	0.04	45.7	5114	1.80 ± 0.12	11.4 ± 4.4	2.5 ± 0.8
3FGL J0528.3+1815	82.11	18.27	0.04	35.7	9388	1.67 ± 0.15	6.6 ± 3.6	2.6 ± 1.1
3FGL J0620.4+2644	95.17	26.74	0.02	92.0	17855	1.54 ± 0.11	6.3 ± 2.8	5.2 ± 1.6
3FGL J0640.0-1252	100.01	-12.90	0.02	174.1	15629	1.52 ± 0.09	10.3 ± 3.4	9.1 ± 2.3
3FGL J0646.4-5452	101.62	-54.92	0.03	190.3	1808	1.46 ± 0.19	8.8 ± 1.8	1.5 ± 0.2
3FGL J0648.1+1606	102.03	16.09	0.03	40.1	7506	1.82 ± 0.16	10.7 ± 5.9	2.1 ± 0.7
3FGL J0650.5+2055	102.64	20.93	0.02	206.2	5767	1.72 ± 0.08	21.9 ± 5.7	6.8 ± 1.6
3FGL J0733.5+5153	113.35	51.86	0.03	104.3	6571	1.69 ± 0.10	9.9 ± 3.2	3.7 ± 1.1
3FGL J0742.4-8133c	115.45	-81.54	0.05	32.3	3120	2.03 ± 0.28	21.1 ± 15.4	1.7 ± 0.6
3FGL J0746.9+8511	117.25	85.22	0.03	119.0	5610	1.68 ± 0.09	10.0 ± 2.8	3.9 ± 1.1
3FGL J0921.0-2258	140.24	-22.95	0.03	62.5	5942	1.74 ± 0.14	9.4 ± 4.1	2.7 ± 1.0
3FGL J1040.8+1342	160.26	13.72	0.03	69.1	6670	1.71 ± 0.12	8.3 ± 3.4	2.7 ± 1.0
3FGL J1141.2+6805	175.33	68.08	0.02	140.1	5131	1.69 ± 0.09	10.9 ± 2.8	4.0 ± 1.1
3FGL J1155.4-3417	178.87	-34.33	0.02	147.3	6825	1.64 ± 0.09	11.8 ± 3.3	5.7 ± 1.6
3FGL J1158.9+0818	179.71	8.31	0.04	51.5	4579	1.81 ± 0.14	11.0 ± 4.6	2.2 ± 0.8
3FGL J1203.5-3925	180.85	-39.42	0.03	103.2	6994	1.70 ± 0.10	13.5 ± 4.5	4.7 ± 1.3
3FGL J1319.6+7759	199.95	78.01	0.02	182.6	2448	1.95 ± 0.08	28.3 ± 5.9	3.1 ± 0.6
3FGL J1434.6+6640	218.72	66.67	0.03	73.9	7426	1.58 ± 0.12	4.4 ± 1.7	2.8 ± 1.1
3FGL J1446.8-1831	221.75	-18.51	0.05	27.9	7841	1.71 ± 0.15	6.1 ± 3.3	2.1 ± 0.9
3FGL J1547.1-2801	236.81	-28.04	0.03	96.8	6165	1.78 ± 0.09	19.0 ± 6.1	4.5 ± 1.1
3FGL J1612.4-3100	243.10	-30.99	0.02	495.0	2091	1.86 ± 0.08	38.0 ± 7.8	5.4 ± 0.5
3FGL J1714.1-2029	258.52	-20.48	0.03	73.8	25559	1.44 ± 0.15	5.1 ± 2.3	7.0 ± 2.2
3FGL J1711.6+8846	258.67	88.75	0.04	44.3	5023	1.83 ± 0.12	8.8 ± 4.2	1.6 ± 0.6
3FGL J1824.4+4310	276.12	43.18	0.03	80.9	5687	1.83 ± 0.12	13.6 ± 5.3	2.5 ± 0.7
3FGL J1841.2+2910	280.36	29.16	0.02	195.9	5355	1.80 ± 0.08	29.0 ± 7.1	6.2 ± 1.2
3FGL J1855.1-6008	283.67	-60.13	0.06	21.4	5051	1.84 ± 0.16	7.2 ± 3.9	1.3 ± 0.6
3FGL J1908.8-0130	287.20	-1.53	0.02	306.4	2468	1.52 ± 0.21	18.6 ± 2.8	4.1 ± 0.4
3FGL J1910.8+2855	287.71	28.94	0.02	102.3	9826	1.62 ± 0.10	9.8 ± 3.3	5.1 ± 1.4
3FGL J1939.6-4925	294.96	-49.47	0.03	64.6	4276	1.85 ± 0.11	14.9 ± 5.0	2.6 ± 0.7
3FGL J1944.1-4523	296.11	-45.38	0.02	100.7	9091	1.64 ± 0.10	9.4 ± 3.3	4.5 ± 1.3
3FGL J1959.8-4725	299.94	-47.43	0.01	923.8	2667	1.52 ± 0.08	30.5 ± 5.0	8.5 ± 1.0
3FGL J2108.6-8619	316.99	-86.31	0.03	91.0	8505	1.65 ± 0.12	10.3 ± 4.0	4.6 ± 1.5
3FGL J2312.9-6923	348.40	-69.39	0.04	35.3	6111	1.72 ± 0.17	5.5 ± 2.9	1.7 ± 0.8
3FGL J2316.8-5209	349.28	-52.19	0.06	37.3	3463	1.89 ± 0.16	10.8 ± 5.0	1.5 ± 0.6
3FGL J2347.9+5436	356.97	54.58	0.02	163.0	5858	1.79 ± 0.08	24.2 ± 6.4	5.4 ± 1.1
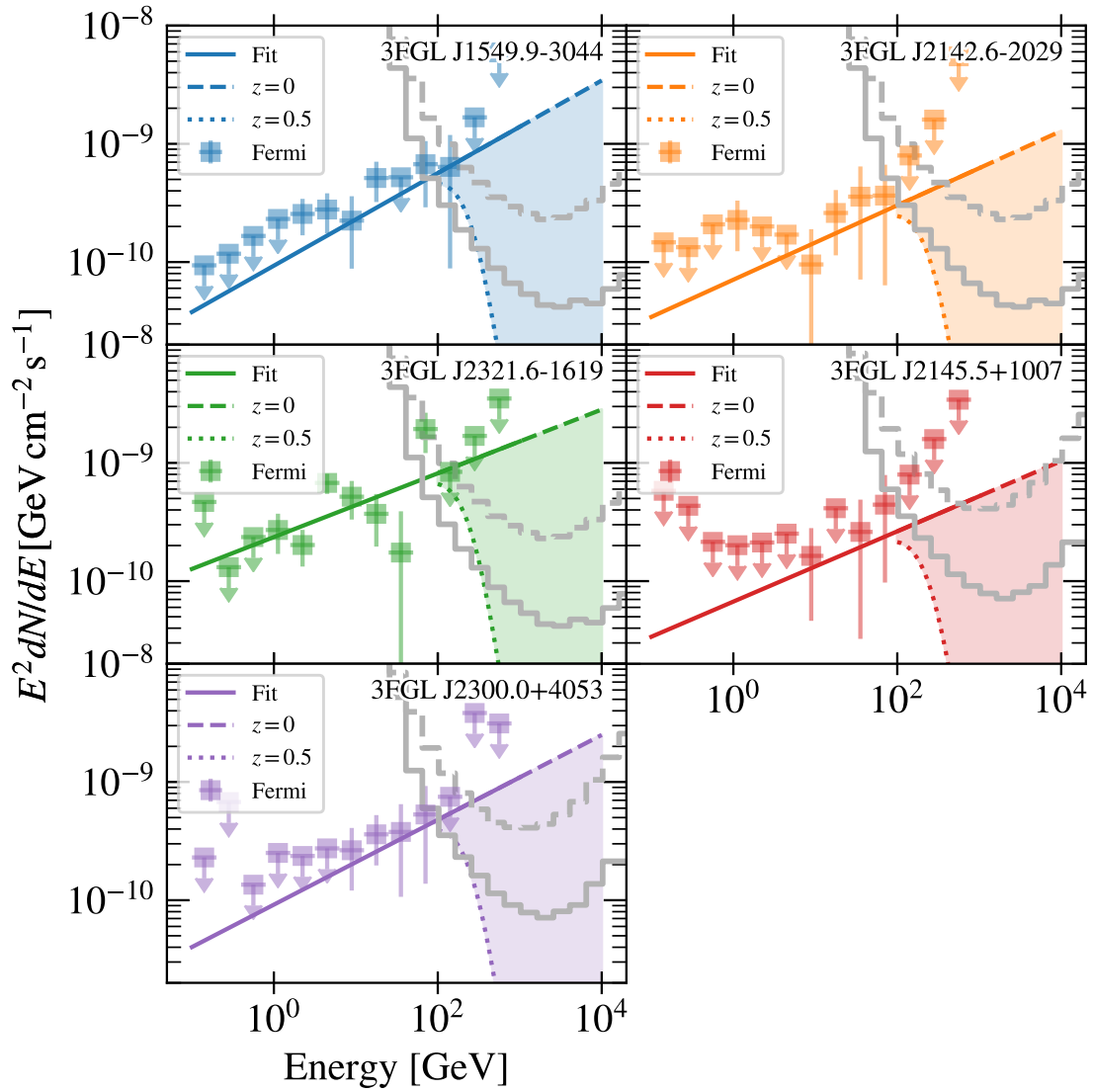
Figure 3. SEDs of the VHC UCS sources as TeV candidates. The dashed (dotted) line denotes the extrapolation of the best-fit spectra up to 10 TeV for a redshift of $z = 0$ ($z = 0.5$) The shaded region indicates the possible source flux for redshifts between $0 < z \leq 0.5$. The CTA sensitivity for 5 (50) hours of observation is shown as a gray dashed (solid) line.

Table 4. Same as Table 3 for UCS$_{agn}$ HSP candidates.

3FGL name	RA	DEC	pos_{68}%	TS	Pivot Energy	Sp.Index	Flux	Energy Flux
	[deg]	[deg]	[deg]		MeV		[10^{-9} ph/cm^2/s]	[10^{-6} MeV/cm^2/s]
3FGL J0020.9+0323	5.26	3.36	0.04	60.7	2545	2.01 ± 0.14	23.3 ± 8.4	2.1 ± 0.5
3FGL J0049.0+4224	12.26	42.38	0.04	37.0	6743	1.81 ± 0.16	8.1 ± 4.4	1.7 ± 0.6
3FGL J0234.2-0629	38.59	-6.47	0.03	90.7	3885	1.83 ± 0.11	15.6 ± 4.8	2.9 ± 0.8
3FGL J0251.1-1829	42.79	-18.50	0.02	104.3	6889	1.59 ± 0.10	7.0 ± 2.2	4.3 ± 1.4
3FGL J0312.7-2222	48.15	-22.36	0.02	177.1	3384	1.84 ± 0.08	22.3 ± 5.2	3.9 ± 0.9
3FGL J0506.9+0321	76.71	3.38	0.03	77.1	5921	1.81 ± 0.12	15.3 ± 6.0	3.0 ± 0.9
3FGL J0524.5-6937	81.16	-69.61	0.03	94.1	3485	2.05 ± 0.15	49.4 ± 21.2	3.8 ± 0.7
3FGL J0527.3+6647	81.86	66.80	0.03	51.9	4664	1.91 ± 0.15	13.0 ± 6.0	1.7 ± 0.5
3FGL J0731.8-3010	112.96	-30.13	0.04	37.1	4523	1.96 ± 0.17	22.4 ± 11.9	2.4 ± 0.7
3FGL J0813.5-0356	123.45	-3.95	0.04	57.0	6101	1.71 ± 0.12	9.1 ± 3.5	3.0 ± 1.1
3FGL J0928.3-5255	142.09	-52.94	0.02	98.7	4267	2.09 ± 0.09	88.0 ± 25.5	6.0 ± 0.9
3FGL J0952.8+0711	148.22	7.23	0.04	51.0	3731	1.92 ± 0.15	14.0 ± 6.0	1.8 ± 0.6
3FGL J1057.6-4051	164.43	-40.87	0.03	40.2	7420	1.72 ± 0.15	6.6 ± 3.4	2.1 ± 0.9
3FGL J1155.3-1112	178.82	-11.19	0.03	52.5	2876	2.03 ± 0.22	21.2 ± 8.9	1.8 ± 0.5
3FGL J1222.7+7952	185.92	79.90	0.04	43.8	2784	2.13 ± 0.22	21.1 ± 12.1	1.3 ± 0.3
3FGL J1225.4-3448	186.35	-34.75	0.05	22.3	7527	1.74 ± 0.19	5.1 ± 3.4	1.5 ± 0.7
3FGL J1234.7-0437	188.71	-4.56	0.04	51.5	3563	2.01 ± 0.14	23.5 ± 9.7	2.1 ± 0.5
3FGL J1513.3-3719	228.35	-37.39	0.03	54.7	4817	1.94 ± 0.13	19.8 ± 8.4	2.3 ± 0.6
3FGL J1525.8-0834	231.53	-8.53	0.03	59.5	3993	1.92 ± 0.12	20.0 ± 7.3	2.5 ± 0.6
3FGL J1528.1-2904	232.12	-29.11	0.06	26.3	7353	1.80 ± 0.18	8.7 ± 5.4	1.8 ± 0.8
3FGL J1545.0-6641	236.21	-66.71	0.02	150.1	11249	1.60 ± 0.10	11.2 ± 3.9	6.6 ± 1.8
3FGL J1549.9-3044	237.46	-30.75	0.02	64.3	9844	1.61 ± 0.12	6.2 ± 2.6	3.5 ± 1.2
3FGL J1619.1+7538	244.78	75.61	0.02	107.1	3836	1.87 ± 0.10	15.5 ± 4.7	2.4 ± 0.6
3FGL J1922.2+2313	290.57	23.25	0.03	80.8	2942	2.22 ± 0.14	93.1 ± 36.7	4.5 ± 0.7
3FGL J2015.3-1431	303.81	-14.55	0.06	17.4	8312	1.81 ± 0.21	5.6 ± 4.2	1.1 ± 0.5
3FGL J2043.6+0001	310.94	0.00	0.04	48.5	2753	2.02 ± 0.14	21.5 ± 8.1	1.9 ± 0.5
3FGL J2053.9+2922	313.45	29.37	0.02	359.6	5647	1.77 ± 0.06	46.0 ± 8.4	11.5 ± 1.7
3FGL J2142.6-2029	325.66	-20.50	0.04	36.1	7683	1.69 ± 0.17	5.0 ± 2.9	1.9 ± 0.9
3FGL J2145.5+1007	326.38	10.13	0.03	34.1	10875	1.70 ± 0.20	4.8 ± 3.4	1.6 ± 0.8
3FGL J2224.4+0351	336.12	3.89	0.05	29.5	2865	1.94 ± 0.18	13.2 ± 6.4	1.5 ± 0.6
3FGL J2300.0+4053	345.06	40.88	0.03	52.5	8886	1.64 ± 0.14	6.2 ± 3.0	2.9 ± 1.2
3FGL J2309.0+5428	347.20	54.41	0.03	77.1	7135	1.75 ± 0.10	16.2 ± 5.7	4.4 ± 1.2
3FGL J2321.6-1619	350.40	-16.32	0.02	174.5	4141	1.73 ± 0.08	17.3 ± 4.1	5.2 ± 1.3

[239] Hoecker, A., Speckmayer, P., Stelzer, J., et al. ,2007, ArXiv Physics 0703039

[241] Kolmogorov A., 1933, G. Ist. Ital. Attuariale 4, 83

[242] Kashlinsky A. et al.,2005, 409,361

[243] Lefaucheur J., Pita S. 2007, A&A, 602,86

[244] Lott B. , Escande, L., Larsson, S et al., 2012, A&A, 544, A6

[245] Massaro F., Paggi A. , Errando M. et al., 2013, ApJS, 207,16

[247] Massaro F. , Landoni R. D'Abrusco D. et al.,2015,A&A, 24, 2

[249] Nikisov A., 1962, Sov.Phys., 14,393

[250] Padovani P., Giommi P., Rau A., 2012, MNRAS, 422, 48

[251] Pita S. , 2017, AIPC, 1792,25

[252] Richard M. P., and Lippman R. P., 1991, Neural Computation, 3, 461

[254] Rieger F.M. , Wilhelmi, E., Aharonian A. et al, 2013, FrPhy, 8, 714

[256] Rumelhart, D. E., Hinton, G. E., Williams, R. J. 1986, Nature

[258] Saz Parkinson P., Xu H., Yu P. et al, (2016), ApJ, 820,2

[259] Salvetti D. Chiaro G. , La Mura G. et al., 2017, MNRAS, 470, 1291

[261] Wilks S.S., 1938, AMS, 9, 60

[262] Wood M., Caputo R., Charles E. et al. 2017, ArXiv: 1707.09551

Chiaro et al.

Table 5. Maximum redshift values so that the BCU VHC and UCS$_{agn}$ VHC are still detectable at $5\,\sigma$ in a 5 (50) hours of CTA (current IACT) observation. If no value is given, the source will not be significantly detected with the assumed observation time.

3FGL name	$z_{\max}$ ($T_{\mathrm{obs}} = 5$ hours)	$z_{\max}$ ($T_{\mathrm{obs}} = 50$ hours)
BCU HC$_{TeV}$ candidates		
3FGL J0047.9+5447	0.15	> 0.50
3FGL J1155.4-3417	0.40	> 0.50
3FGL J1434.6+6640	0.13	> 0.50
3FGL J0921.0-2258	0.11	> 0.50
3FGL J0648.1+1606	0.01	0.29
3FGL J1711.6+8846	—	0.22
3FGL J1714.1-2029	> 0.50	> 0.50
3FGL J1910.8+2855	0.25	> 0.50
3FGL J0153.4+7114	0.08	> 0.50
3FGL J0506.9-5435	> 0.50	> 0.50
3FGL J1944.1-4523	0.29	> 0.50
UCS$_{agn}$ HC$_{TeV}$ candidates		
3FGL J1549.9-3044	0.21	> 0.50
3FGL J2142.6-2029	0.08	0.42
3FGL J2321.6-1619	0.31	> 0.50
3FGL J2145.5+1007	0.02	0.26
3FGL J2300.0+4053	0.12	> 0.50